Synthesis of $Cs_3Cu_2I_5$ Nanocrystals in a Continuous Flow System

Ksenija Arslanova[1,4], Patrick Ganswindt*[1], Tizian Lorenzen[2], Ekaterina Kostyurina[3], Konstantin Karghiosoff [4], Bert Nickel[3], Knut Müller-Caspary[2], Alexander S. Urban*[1]

January 2024

Affiliations

[1] K. Arslanova (ksenija.arslanova@unibw.de)
P. Ganswindt (p.ganswindt@physik.lmu.de)
A. S. Urban (urban@lmu.de)
Nanospectroscopy Group and Center for NanoScience
Faculty of Physics
Ludwig-Maximilians-Universität München
Königinstr. 10, 80539 München, Germany

[2] T. Lorenzen (t.lorenzen@campus.lmu.de)
K. Müller-Caspary (k.mueller-caspary@cup.lmu.de)
Department of Chemistry and Center for NanoScience
Ludwig-Maximilians-Universität München
Butenandtstr. 11, 81377 München, Germany

[3] E. Kostyurina (E.Kostyurina@physik.uni-muenchen.de)
B. Nickel (nickel@lmu.de)
Soft Condensed Matter Group and Center for NanoScience
Faculty of Physics
Ludwig-Maximilians-Universität München
Geschwister-Scholl-Platz 1, 80539 München, Germany

[4] K. Karaghiosoff (Konstantin.karaghiosoff@cup.uni-muenchen.de)
Faculty of Chemistry and Pharmacy
Ludwig-Maximilians-University München
Butenandtstr.5-13, Haus D, 81377 München, Germany

Keywords

Ternary copper halides, continous flow synthesis, flow chemistry, synthesis optimization, morphology control

Abstract

Achieving the goal of generating all of the world's energy via renewable sources and significantly reducing our energy usage will require the development of novel abundant, nontoxic energy conversion materials. Here, we develop a cost-efficient and scalable continuous flow synthesis of $Cs_3Cu_2I_5$ nanocrystals as a basis for the rapid advancement of novel nanomaterials. Ideal precursor solutions were obtained through a novel batch synthesis, whose product served as a benchmark for the subsequent flow synthesis. Realizing this setup enabled

1

a reproducible fabrication of $Cs_3Cu_2I_5$ nanocrystals. We determined the effect of volumetric flow rate and temperature on the final product's morphology and optical properties, obtaining 21 % quantum yield with the optimal configuration. Consequently, we can tune the size and morphology of the nanocrystals with far more precision and in a much wider range than previously achievable. The flow setup is easily applicable to other relevant nanomaterials. It should enable a rapid determination of a material's potential and subsequently optimize its desired properties for renewable energy generation or efficient optoelectronics.

Introduction

Ternary copper halide nanocrystals (NC) have been attracting growing attention as an alternative to lead-based halide perovskites for a broad range of optoelectronic applications.[1] Their 0D crystal structure and self-trapped exciton (STE) mediated emission often lead to high photoluminescence quantum yields (PLQYs) with outstanding stability at elevated temperatures and upon exposure to moisture. (The term "0D" crystal structure refers to the isolated nature on the molecular level of the copper iodide complexes - edge sharing dimers of tetrahedral and triagonal planar copper iodide complexes.)[2–4] One such material, $Cs_3Cu_2I_5$ nanocrystals, has exhibited a large potential for a broad range of optoelectronic applications, such as deep-blue light-emitting diodes (LEDs), ultraviolet (UV) photodetectors or as fluorescent inks for encryption technologies.[5–7] While several syntheses have been developed for these exciting nanocrystals, scalability and morphological control over the reaction products are still major obstacles for this material class.[1,8,9] Reaction temperature has been determined to influence the nanocrystal geometry in hot-injection syntheses, with a transition from small spheres to larger anisotropic nanorods with increasing temperature.[10] In the first implementation of a fully autonomous and self optimizing continuous-flow based synthesis, the CuI-precursor concentration and reaction temperature were determined to be the most influential parameters for the synthesis.[11] While the 0D crystal structure of the material precludes quantum confinement effects due to nanocrystal size, a dependency of the PLQY on the size of the nanocrystals was previously observed and attributed to the number of surface defects, highlighting the need for controlled surface coordination by ligands.[9] Employing continuous flow systems for the fabrication of semiconductor nanocrystals has the dual advantage of having more precise control over reaction parameters and being able to screen reaction conditions significantly faster, employ more moderate reaction conditions and lower precursor concentration due to increased heat- and mass-transfer as well as easily scale up the material production due to the continuous nature of the procedure.[12] In the following, we present a facile and low-cost single-phase continuous flow approach for the synthesis of $Cs_3Cu_2I_5$ nanocrystals. To obtain ideal precursors for this synthesis and to serve as a material baseline, we initially developed a novel hot-injection batch synthesis, which can be performed under ambient conditions. Based on this approach, we investigated a series of different preparation methods for synthesizing $Cs_3Cu_2I_5$ nanocrystals under continuous flow conditions. After establishing a reliable and reproducible synthesis protocol, we systematically investigated the influence of the flow rate and the reaction temperature on the optical properties and morphology of the $C_3Cu_2I_5$ NCs. The volumetric screenings reveal a direct dependence of the nanocrystal size on the flow rate and a transition in morphology from spherical particles to nanorods with increasing reaction temperature. Furthermore, we are able to optimize the nanocrystals' optical quality, as gauged by their PLQY, which reached the levels achieved through batch synthesis. This facile approach is easily applicable to other materials and should help to rapidly identify and optimize novel materials with higher potential for renewable energy generation and efficient energy usage.
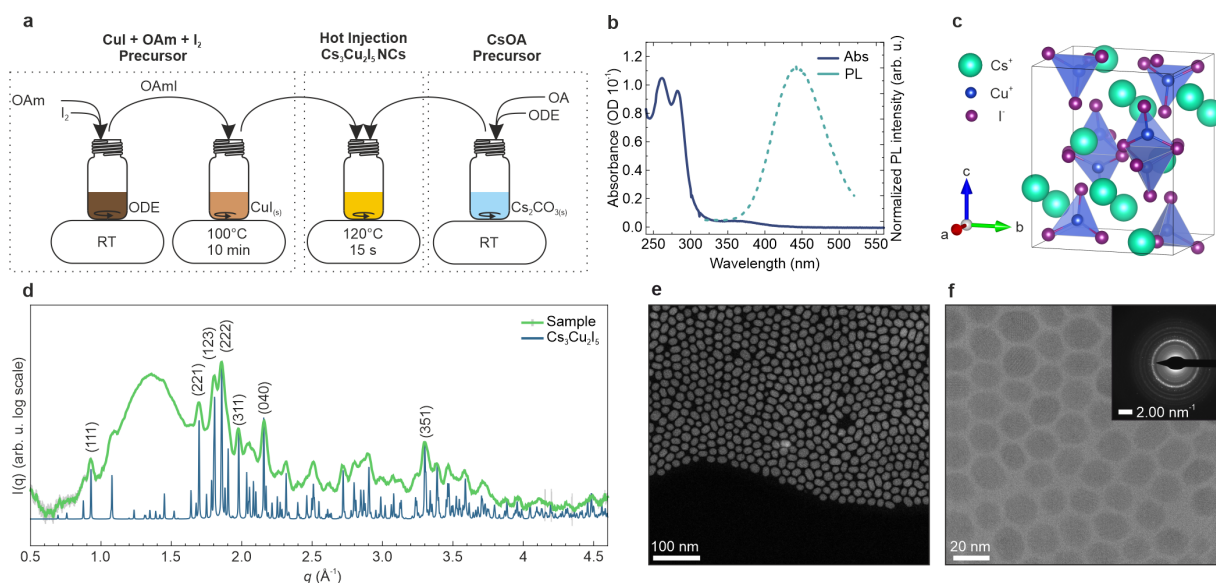
Results and Discussion

Figure 1: a) Schematic depiction of the hot-injection batch synthesis, showing the separate preparation of the copper precursor (left) and cesium precursor (right). b) Absorbance and normalized photoluminescence spectra of the obtained $Cs_3Cu_2I_5$ nanocrystal dispersion. The photoluminescence was normalised to the optical density (OD) of the sample at the excitation wavelength of 280 nm. c) Simplified depiction of the 0D crystal structure of $Cs_3Cu_2I_5$. d) Powder X-ray diffractogram showing sample diffraction in green and theoretical reference in blue.[13] e) HR-STEM image and f) HR-TEM image of the nanocrystals with corresponding electron diffraction.

As a prerequisite to establishing a continuous flow synthesis for $Cs_3Cu_2I_5$ nanocrystals, a batch synthesis was required to serve as a basis for designing the continuous flow reactor and to provide a reference to assess the viability of the flow integration. With only a limited number of viable batch syntheses in air reported, a novel batch, hot-injection approach for the synthesis of $Cs_3Cu_2I_5$ nanocrystals based on the direct use of copper(I) iodide in the presence of oleylamine (OAm) and iodine was developed.[7–9,14] As outlined in Figure 1, the synthesis exploits an in situ formation of oleylammonium iodide (OAmI) as an external iodide source and dissolution agent for CuI as previously reported.[15] The excess iodide concurrently serves as a reducing agent, suppressing the undesired formation of copper(II) salts and allowing the use of the precursor solution outside of a glove box.[9] For the hot-injection synthesis, a cesium oleate precursor in 1-octadecene (ODE) and the copper precursor (CuI + OAm+ I_2) were separately heated to 120 °C. The copper precursor was then rapidly injected into the cesium oleate solution, vigorously stirred for 15 s and then immediately cooled to 0 °C with an ice-water bath. The reaction mixture was then purified before characterization (see Supporting Information for details). UV-Vis spectroscopy reveals a strong absorption in the UV range, with two prominent peaks at 263 nm and 282 nm, the latter being attributed to excitonic absorption (Figure 1 b). The photoluminescence (PL) spectra reveal a single, broad (full width at half maximum (FWHM) of 80 nm) emission peak centered at 440 nm, both indicative of STE emission.[7,14] The sample possesses a robust PLQY of 21.7 %, a respectable value in light of the reported size dependence of the PLQY for this material.[9] Powder X-ray diffraction (PXRD) confirmed the material to be $Cs_3Cu_2I_5$, which crystallizes in the space group Pnma (No.62) (Figure 1 c,d). No undesired secondary phases, such as CsI or CuI were detected, a testament to the purity and high quality of the sample (see Figure S1).[16–18] High-resolution scanning transmission electron microscopy (HR-STEM) shows the material to comprise regular, round, and partially elongated nanocrystals with an average diameter of 17.3 nm (Figure 1 e). The electron diffraction pattern obtained from high-resolution transmission electron microscopy (HR-TEM) revealed some of the material's lattice planes, which correlated with theoretical values, further confirming the crystal structure (Figure 1 f, Table S1).[16] The nanocrystals displayed excellent stability, with the optical properties and morphology preserved after storage under ambient conditions for 6 months (see Figure S2).

Based on the developed hot-injection batch approach, we designed a continuous flow system, composed of two precursor syringes, separate pre-heating loops, a Y-inlet for precursor mixing combined with a heated coil reactor (T_1), and a cooling section (T_2) with subsequent sample collection as shown in Figure 2 a (for a more detailed description of the continuous flow integration see section Sections S1 and S2). We adopted a single-phase flow approach to minimize system complexity by achieving precursor mixing at the Y-inlet and in the coiled reactor.[19] To avoid precipitation inside the syringes or clogging of the flow system, we modified the precursor
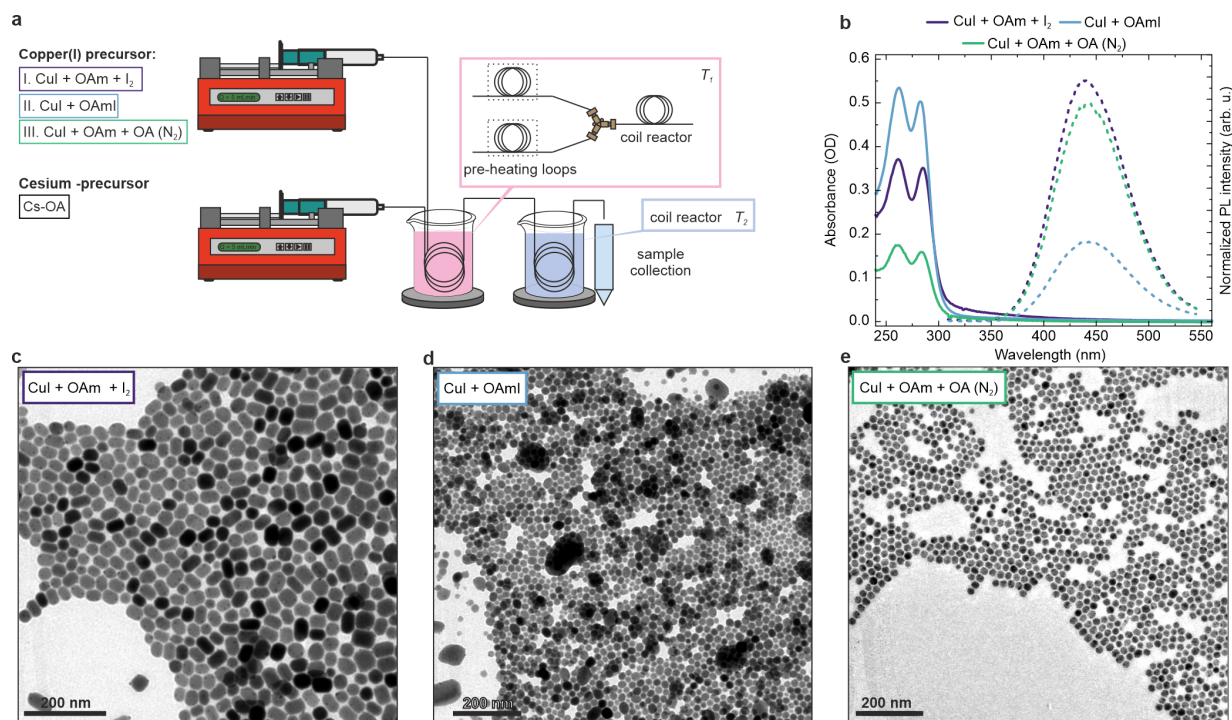
4

Figure 2: a) Schematic of the developed flow setup and the employed precursor solutions. b) Corresponding absorbance and relative photoluminescence of the samples prepared from the three different precursors. c-e) BF-TEM images of the respective nanoparticles obtained from the different precursor approaches.

solutions from those used in the batch synthesis.[20] To facilitate stability at room temperature, we adjusted the concentration of both precursor solutions to $0.01\,M$ and increased the OA content in the cesium-precursor (to a Cs:OA ratio of 1:13).[8] The resulting material was collected and purified before further characterization (see Section S2). As shown in Figure 2 b, the resulting product exhibited the same qualitative optical properties of the material obtained from the batch synthesis. The optical density at the excitation wavelength of $280\,nm$ of the continuous flow sample after identical purification is an order of magnitude higher than the batch sample, indicating an improved reaction yield. The sample emits strong PL, confirmed by a PLQY of over $27.8\,\%$, signifying both excellent quality and purity of the in-flow prepared nanocrystals. TEM micrographs show regular nanocrystals with an elongated shape, similar to the batch synthesis (Figure 2 c), with an average size of $24\,nm$, roughly an order of magnitude smaller than previously achieved with other continuous flow systems.[11] Dynamic light scattering measurements confirm the monodisperse nature of the sample with only a single particle species present (see Figure S3). Despite these impressive results, the procedure suffered from reproducibility issues, likely caused by the copper-precursor solution (for a detailed explanation, see Section S2). Accordingly, despite this being the first time that colloidally stable $Cs_3Cu_2I_5$ NCs could be successfully synthesized from a single-phase continuous flow setup, we excluded the use of this precursor solution for further investigation of the system.

As determined previously, OAmI is responsible for the dissolution and stabilization of CuI in the precursor solution and the nanocrystals obtained after the synthesis.[15] Consequently, to circumvent the issues encountered with the first precursor, OAmI was synthesized according to a modified approach from Maceiczyk et. al. and directly employed in a stoichiometric ratio of 2:3 between CuI and OAmI as the second precursor to be assessed for the continuous flow synthesis (Figure 2 a, Section S2, Table S2).[21] The ratio was crucial to overcome the low solubility of CuI in 1-octadecene. The synthesis also yielded regular nanocrystals Figure 2 d with the characteristic optical properties (light blue graphs in Figure 2 b), confirming the desired $Cs_3Cu_2I_5$ composition. However, the low relative PL intensity and a PLQY of only $2.8\,\%$ indicate poor optical quality. The TEM micrographs also showed a significant presence of impurities, likely excess OAmI in the precursor solution. Furthermore, the nanocrystal dispersion displayed poor stability, precipitating under ambient conditions after $24\,h$, also eliminating this precursor for further investigation (see also Figure S6). The quality and reproducibility issues of the first two precursors likely stemmed from using an external iodide source or the excess ligand necessary. Thus, we prepared the copper and cesium precursors separately under inert conditions with a Schlenk line.[11] Without an external iodide source and in the absence of ambient oxygen, the copper(I) precursor could directly be prepared at the required dilute concentrations and remained stable at room temperature (see Section S2). Using this precursor, the resulting nanocrystals are extremely homogeneous (Figure 2 e),
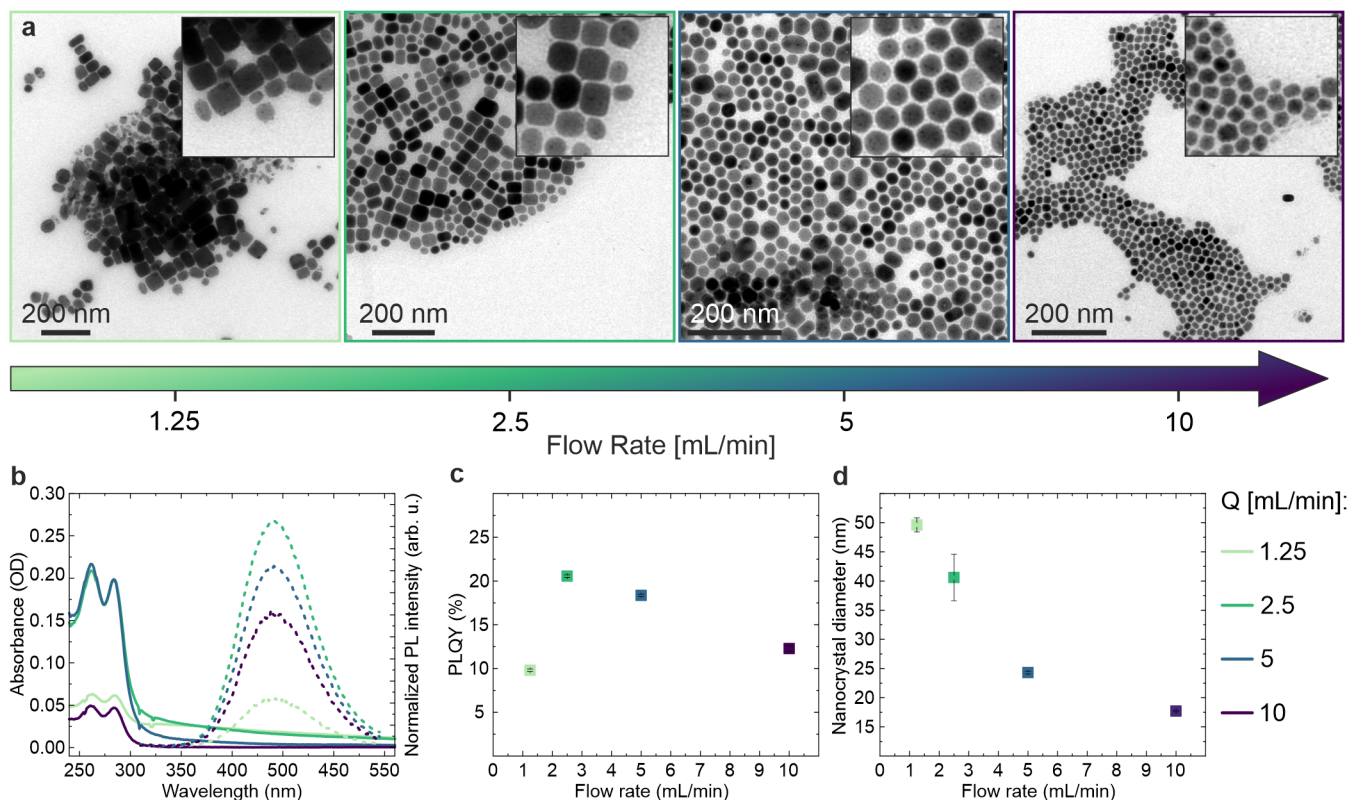
5

Figure 3: a) TEM micrographs of samples prepared at different flow rates with a reaction temperature of 75 °C. b) Absorbance and normalized PL intensity of the corresponding dispersions. c) PLQY of all samples investigated in the flow rate screening. d) Average size of the obtained nanocrystals diameters as determined from the TEM micrographs.

with an average size of 23.4 nm. The optical properties align with the previous syntheses (turquoise graphs in Figure 2 b), with a low optical density at 280 nm likely due to the smaller size of the NCs and possibly lower reaction yields. However, the high relative PL intensity and a PLQY of 18.7 % indicate excellent material quality. Most importantly, the resulting nanocrystals were extremely stable, and the method was highly reproducible, yielding nearly identical results between different syntheses. Further characterization confirmed the high quality and purity of the sample: HR-STEM and electron diffraction confirmed the crystallinity of the nanoparticles and the theoretical lattice spacings of the desired 0D $Cs_3Cu_2I_5$ phase (see Figure S7). Energy-dispersive X-ray spectroscopy (EDX) mapping of the particles revealed a homogeneous distribution of all elements (Figure S8) and PXRD analysis did not detect any significant amount of impurities (Figure S9). These results confirm that operating in a stochiometric excess of copper has a positive influence on the quality of the NCs. [10,11]

Having established a successful and reliable continuous flow synthesis, we turned to optimizing the resulting $Cs_3Cu_2I_5$ nanocrystals. The most important parameters are the reactor temperature and the overall flow rate, which controls the total residence time. This is inversely proportional to the volumetric flow rate, Q, in $mL\,min^{-1}$ and is given by $t_{synth} = C/Q$, with a constant $C = 50\,s \cdot mL\,min^{-1}$ (employed flow rates and residence times are listed in Table S5). To understand how the nanocrystals grow, we varied the flow rate from 1.25-10 $mL\,min^{-1}$, corresponding to residence times of 40-5 s at a reaction temperature of 75 °C (Figure 3 a-d). At 10 $mL\,min^{-1}$ (t_{synth} =5 s), the resulting NCs are slightly irregularly shaped, exhibiting a homogeneous size of only 17 nm, significantly smaller than the nanocrystals obtained in the batch synthesis. The UV-Vis spectrum displays the expected two peaks, with nearly no absorbance at higher wavelengths; however, the absorbance overall is quite low. The PL was clearly detectable with a PLQY of 12.3 %. Increasing the synthesis time to 10 s (5 $mL\,min^{-1}$) leads to far more regular, hexagonal to nearly spherical nanocrystals with an increased size of 24 nm. The absorbance increases nearly fourfold with only a small shoulder on the long wavelength side. The dispersions are also significantly brighter and exhibit a PLQY of 18.3 %. A further increase of the residence time to 20 s (2.5 $mL\,min^{-1}$) leads to a significant increase of the nanocrystal size to 40 nm, with a pronounced size dispersion and a shape change toward a cubic shape. The absorbance is nearly identical in the UV range compared to the previous sample; however, the absorbance increases notably for $\lambda > 300nm$. These nanocrystals also exhibit a further increase in PLQY up to 20.6 %, on par with the batch synthesis value. At the longest synthesis time (40 s), the nanocrystals grow further; however, it becomes difficult to determine
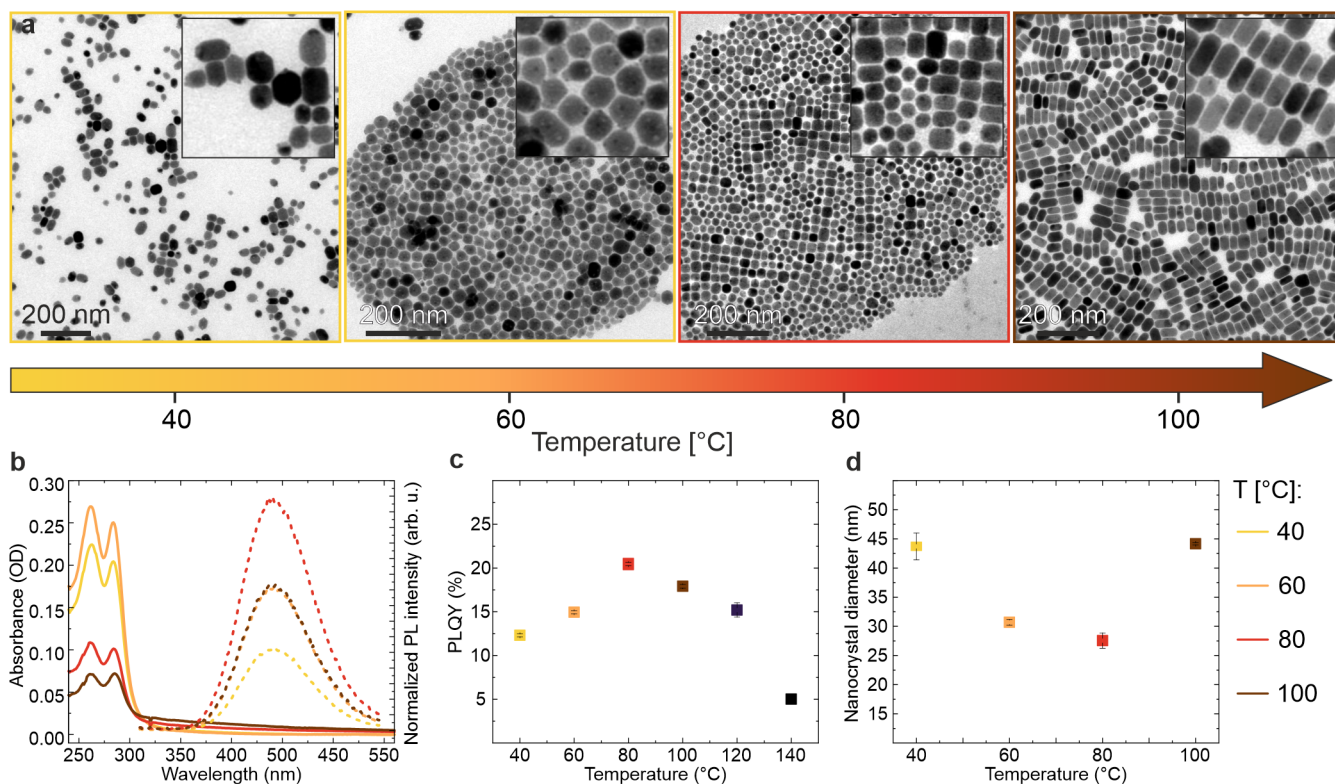
Figure 4: a) TEM micrographs of samples prepared at different T_1 reactor temperatures with a flow rate of $5\,\mathrm{mL\,min^{-1}}$. b) Absorbance and normalized PL intensity of the corresponding dispersions. c) PLQY of all samples investigated in the temperature screening. d) Average size of the obtained nanocrystals diameters as determined from the TEM micrographs.

the exact size as they appear to aggregate. This coincides with a significantly diminished absorbance in the UV (while the long wavelength shoulder remains large) and a diminished PL intensity with a PLQY of only 9.8 %.

Overall, the flow rate screening reveals an increase in nanocrystal size and a transition from predominantly spherical and hexagonal to rectangular and cubic morphology with increasing synthesis time (decreasing flow rate). Additionally, absorbance and PLQY increase initially before declining at the lowest flow rate. As the average nanocrystal size increases only by ca. 7 nm between 5 s and 10 s residence time ($10\,\mathrm{mL\,min^{-1}}$ and $5\,\mathrm{mL\,min^{-1}}$), yet the absorbance increases by a factor of 4, nucleation appears to be dominating the reaction during the first 10 s. This matches a previous study that found slow initial growth periods for $Cs_3Cu_2I_5$ nanorods from batch syntheses.[10] After 20 s residence time ($2.5\,\mathrm{mL\,min^{-1}}$), the average diameter increases by 16 nm while the absorbance remains identical, showing that growth dominates after the first 10 s of nucleation. Extending the residence time to 40 s ($1.25\,\mathrm{mL\,min^{-1}}$), growth stagnates at longer reaction times while colloidal stability and sample quality concurrently deteriorate substantially. The results of this measurement series can be used to target specific nanocrystal sizes while keeping the optical properties nearly constant by simply adjusting the flow rate.

With the ideal flow rate determined, we turned to the second crucial parameter, the temperature. Setting the flow rate to $5\,\mathrm{mL\,min^{-1}}$, we varied the synthesis temperature between 40 and 140 °C. At 40 °C, the nanocrystals display morphologies ranging from spheres and cubes to elongated hexagons, with an average diameter (44 nm) almost twice as large as the nanocrystals obtained at 75 °C in the flow rate screening (Figure 4 d, Figure S13). While the high absorbance indicates a moderate reaction yield, the weak relative PL intensity and PLQY of 12.3 % of the sample indicate poor material quality (Figure 4 b,c). As the reactor temperature increases, the morphology slowly changes from hexagonal to more cubic nanocrystals, with the average size decreasing significantly up to 80 °C. At 100 °C, the nanocrystals form as predominantly very regular nanorods, with an average size of 23x44 nm. At the two highest temperatures employed, the final dispersion turned turbid, indicating severe material aggregation (Figure S11, Figure S12). This also prevented us from acquiring TEM micrographs of the resulting material. The absorption in the UV range increases slightly up to 60 °C and then drops continuously, while the PLQY reaches a maximum of 20.5 % at 80 °C before dropping off and reaching 5 % at 140 °C.

The temperature screening for the continuous flow synthesis of $Cs_3Cu_2I_5$ nanocrystals indicates that aggre-

7

gate formation or uncontrolled nanocrystal growth occur for either too-low or too-high reaction temperatures. At low temperatures, nucleation appears inhibited, causing the growth of few but large nanocrystals of poor quality. At too high temperatures, an anisotropic growth of the nanocrystals with low yields seems to take place, suggesting a fast growth rates that competes with the nanocrystal nucleation, causing defect-rich nanocrystals to form and limiting the reaction yield. Furthermore, the reaction series demonstrated a clear morphological transition from polydisperse and irregular shapes at low temperatures to more regular, anisotropic morphologies at higher temperatures. Additionally, these experiments revealed a temperature dependence of nucleation and growth rate with the latter being favoured at higher temperatures and the former peaking at an intermediate temperature range around $60\,^\circ$C.

In summary, we have developed a facile and low-cost single-phase continuous flow synthesis for $Cs_3Cu_2I_5$ nanocrystals. As a basis for the flow synthesis, a novel batch procedure was developed that allows the preparation of the material under ambient conditions and with the direct use of CuI as a precursor. The procedure yields highly monodisperse nanocrystals of high optical quality and outstanding stability. Subsequently, a low-cost continuous flow system was developed, and three different copper precursors were assessed, yielding a reliable synthesis of high-quality and homogenous nanocrystals that can be prepared at lower temperatures and with higher PLQYs compared to most batch syntheses and other continuous flow approaches. To gain further insights into the formation of the NCs, a screening of the flow rate and reaction temperature was conducted, revealing a strong dependence of the nanocrystals' size on the flow rate and a change of the morphology from regular spherical nanocrystals to nanorods for increasing reaction temperatures. Furthermore, the screening revealed an optimum for the PLQY, approaching $21\,\%$ for nanocrystal sizes below $20\,$nm. The work highlights the beneficial influence continuous flow manufacturing can have on the quality of semiconductor nanocrystals. Through more precise control over reaction conditions, increased heat and mass transfer and access to shorter reaction times with better overall reproducibility compared to batch syntheses, continuous flow syntheses present a powerful tool for obtaining and investigating high-quality semiconductor nanocrystals, which is crucial for advancing and developing highly efficient energy conversion materials for optoelectronic applications.

Methods

Chemicals

All reagents were used as received without further purification: copper(I) iodide (CuI, for synthesis, Sigma Aldrich), caesium carbonate (Cs_2CO_3, 99%, Sigma Aldrich), 1-octadecene (ODE, 90%, Sigma Aldrich), oleylamine (OAm, 70%, Sigma Aldrich), oleic acid (OA, 90%, Sigma Aldrich), iodine (I_2, sublimed, VWR), hydroiodic acid (HI, 57%, Sigma Aldrich), magnesium sulfate ($MgSO_4$, VWR), sodium chloride (NaCl, VWR), acetone (99.9%, Sigma Aldrich), n-Hexane (97%, Sigma Aldrich), ethyl acetate (EtOAc, VWR).

Hot Injection Batch Synthesis of $Cs_3Cu_2I_5$ Nanocrystals

Preparation of $0.1\,M$ CsOA precursor

Cs_2CO_3 (163 mg, 0.5 mmol) was mixed with OA (4.1 mL, 13 mmol) and 5.9 mL ODE in a glass vial. Then, the vial was heated on a hot plate at 120°C until the caesium salt was completely dissolved. The precursor was cooled down to RT and stored under ambient conditions.

Preparation of $0.4\,M$ OAm/I_2 additive

Iodine (252 mg, 1 mmol) was mixed with OAm (1.66 mL, 5 mmol) and 3.33 mL ODE in a glass vial. The mixture was stirred for approx. 30 min.

Preparation of $0.1\,M$ CuI + OAm + I_2 precursor

To prepare a 0.1 M precursor solution, CuI (190 mg, 1 mmol) was mixed with an OAm/I_2 additive (0.4 M, 2 mL) and 8 mL of ODE in a glass vial. Then, the vial was heated on a hot plate at 120 °C until the copper salt was completely dissolved. The precursor was cooled down to RT and stored under ambient conditions.

Hot injection batch synthesis

1.5 mL of 0.1 M CsOA precursor was mixed with 5 mL ODE and heated to 120 °C. 0.1 M "CuI + OAm + I_2" precursor was heated to 120 °C and then 1mL of the "CuI + OAm + I_2" precursor was rapidly injected into the CsOA/ODE mixture. The reaction mixture was stirred for 15 s before it was cooled down to 0 °C by placing the vial into a water-ice bath. The frozen reaction mixture was then allowed to warm to room temperature, transferred to a Falcon tube, and centrifuged at 5000 rpm for 5 min. The resulting sediment was isolated and resuspended in 2 mL of hexane.

Continuous-flow procedure

Preparation of $0.01\,M$ CsOA precursor

Cs_2CO_3 (163 mg, 0.5 mmol) was mixed with OA (4.1 mL, 13 mmol) and 5.9 mL ODE in a glass vial. Then, the vial was heated on a hot plate at 120 °C until the caesium salt was completely dissolved. The precursor was cooled down to RT and stored under ambient conditions. Before the synthesis, the 0.1 M precursor solution was diluted with ODE 1:9 to obtain a 0.01 M precursor solution.

Preparation of $0.4\,M$ OAm/I_2 additive

Iodine (252 mg, 1 mmol) was mixed with OAm (1.66 mL, 5 mmol) and 3.33 mL ODE in a glass vial. The mixture was stirred for approx. 30 min.

Preparation of $0.01\,M$ CuI + OAm + I_2 precursor

CuI (57 mg, 0.3 mmol) was mixed with an OAm/I_2 additive (0.4 M, 1.125 mL) and 1.875 mL of ODE in a glass vial. Then, the vial was heated on a hot plate at 120 °C until the copper salt was completely dissolved. Before the synthesis, the 0.1 M precursor solution was diluted with ODE 1:9 to obtain a 0.01 M precursor solution.

Preparation of $0.5\,M$ OAmI additive

Oleylammonium iodide was synthesised according to the synthesis of Maceiczyk et al.[21] Oleylamine (12.5 mL, 38 mmol) was dissolved in absolute ethanol (100 mL). The mixture was cooled to 0 °C, and hydroiodic acid (57%, 10 mL, 76 mmol) was added dropwise. The mixture was left to stir overnight at room temperature. Subsequently, the ethanol was removed using a rotary evaporator, and the aqueous phase was extracted with ethyl acetate

https://doi.org/10.26434/chemrxiv-2024-1sx0b ORCID: https://orcid.org/0000-0001-6168-2509 Content not peer-reviewed by ChemRxiv. **License:** CC BY-NC 4.0

($3\times100\,\mathrm{mL}$). The organic phase was washed with brine ($3\times50\,\mathrm{mL}$) and dried over $MgSO_4$. Afterward, the solvent was removed under vacuum. The resulting product was used without further purification. To obtain $0.5\,\mathrm{M}$ OAmI solution in ODE, OAmI ($988.5\,\mathrm{mg}$, $2.5\,\mathrm{mmol}$) was dissolved at $100\,^{\circ}\mathrm{C}$ in $5\,\mathrm{mL}$ ODE.

Preparation of $0.01\,\mathrm{M}$ **CuI + OAmI precursor**

CuI ($38\,\mathrm{mg}$, $0.2\,\mathrm{mmol}$) was mixed with OAmI additive ($0.5\,\mathrm{M}$, $0.6\,\mathrm{mL}$), OAm ($1\,\mathrm{mL}$, $3\,\mathrm{mmol}$), and $1.4\,\mathrm{mL}$ ODE in a glass vial. Then, the vial was heated on a hot plate at $120\,^{\circ}\mathrm{C}$ until the copper salt was completely dissolved. Before the synthesis, the $0.1\,\mathrm{M}$ precursor solution was diluted with ODE 1:9 to obtain a $0.01\,\mathrm{M}$ precursor solution.

Preparation of $0.01\,\mathrm{M}$ **CsOA precursor (N_2)**

Cs_2CO_3 ($32\,\mathrm{mg}$, $0.1\,\mathrm{mmol}$) was mixed with OA ($0.82\,\mathrm{mL}$, $2.6\,\mathrm{mmol}$) and $19.18\,\mathrm{mL}$ ODE in a three-necked round bottom flask. The flask was heated to $120\,^{\circ}\mathrm{C}$ for $1\,\mathrm{h}$ under vacuum and cooled down to RT, resulting in a $0.01\,\mathrm{M}$ CsOA precursor solution.

Preparation of 0.01 M **CuI + OA + OAm precursor (N_2)**

CuI ($38\,\mathrm{mg}$, $0.2\,\mathrm{mmol}$) was mixed with $10\,\mathrm{mL}$ ODE in a three-necked round bottom flask. The flask was heated to $120\,^{\circ}\mathrm{C}$ under vacuum for $30\,\mathrm{min}$ to degas the mixture. Simultaneously, oleic acid ($1\,\mathrm{mL}$, $3\,\mathrm{mmol}$) and oleylamine ($1\,\mathrm{mL}$, $3\,\mathrm{mmol}$) ligands were mixed with $8\,\mathrm{mL}$ ODE in a separate three-necked round bottom flask and degassed at $120\,^{\circ}\mathrm{C}$ under vacuum for $30\,\mathrm{min}$. After that, $10\,\mathrm{mL}$ of OA/OAm/ODE mixture were transferred to the CuI/ODE mixture via a syringe. The resulting precursor solution was heated for a further $30\,\mathrm{min}$ at $120\,^{\circ}\mathrm{C}$ and then cooled down to RT. The $0.01\,\mathrm{M}$ CuI + OA + OAm (N_2) precursor was obtained as a clear solution.

Absorbance and PL spectroscopy

PL spectra and UV-Vis absorbance spectra of purified $Cs_3Cu_2I_5$ nanocrystal dispersions were measured with a commercial FluoroMax-4Plus spectrometer equipped with a xenon arc lamp and an F-3031 transmission accessory (HORIBA Scientific). The excitation wavelength for photoluminescence spectra was set to $280\,\mathrm{nm}$. For PLQY measurements a Quanta-phi integrating sphere was employed and the samples were excited at $300\,\mathrm{nm}$.

Dynamic Light Scattering

Dynamic light scattering (DLS) measurements were performed on a Malvern Zetasizer Pro.

Electron Microscopy

High-resolution STEM and TEM imaging was performed using a probe corrected FEI Titan Themis operated at acceleration voltage $300\,\mathrm{kV}$. STEM images were recorded at a semi-convergence angle of $16.6\,\mathrm{mrad}$ at a camera length of $196\,\mathrm{mm}$ using a Fischione HAADF detector. A Super-X detector was used for EDS imaging. Specimen preparation was carried out by drop casting onto TEM grids (Quantifoil R2/2, $2\,\mathrm{nm}$ ultrathin carbon).

Powder X-ray Diffraction

Powder X-ray diffraction data was collected at the laboratory X-ray scattering setup at the soft condensed matter chair of LMU Munich. The setup uses molybdenum K α radiation ($0.71\,\text{Å}$) of a microfocus X-ray source (Xenos) collimated to a beam size of about $1\times 1\,\mathrm{mm}$. Dispersions of NCs in n-hexane were drop-casted onto adhesive tape (3 M Scotch Magic 810) and measured in transmission mode after drying. The data was collected using a Dectris Pilatus 100K detector.

Bibliography

References

[1] Li, Y. *et al.* Progress in copper metal halides for optoelectronic applications. *Materials Chemistry Frontiers* **5**, 4796–4820 (2021).

[2] Guo, Z. *et al.* All-inorganic copper(i)-based ternary metal halides: promising materials toward optoelectronics. *Nanoscale* **12**, 15560–15576 (2020).

[3] Li, Y. *et al.* Progress in copper metal halides for optoelectronic applications. *Materials Chemistry Frontiers* **5**, 4796–4820 (2021).

[4] Ma, Z. *et al.* Stable yellow light-emitting devices based on ternary copper halides with broadband emissive self-trapped excitons. *ACS Nano* **14**, 4475–4486 (2020).

[5] Wang, L. *et al.* Colloidal synthesis of ternary copper halide nanocrystals for high-efficiency deep-blue light-emitting diodes with a half-lifetime above 100 h. *Nano Letters* **20**, 3568–3576 (2020).

[6] Zhao, X. *et al.* $Cs_3Cu_2I_5$/ZnO heterostructure for flexible visible-blind ultraviolet photodetection. *ACS Applied Materials & Interfaces* **14**, 43490–43497 (2022).

[7] Gao, F. *et al.* Deep-blue emissive $Cs_3Cu_2I_5$ perovskites nanocrystals with 96.6% quantum yield via InI_3-assisted synthesis for light-emitting device and fluorescent ink applications. *Nano Energy* **98**, 107270 (2022).

[8] Li, Y. *et al.* Room temperature synthesis of stable, printable $Cs_3Cu_2X_5$ (X = I, Br/I, Br, Br/Cl, Cl) colloidal nanocrystals with near-unity quantum yield green emitters (X = Cl). *Chemistry of Materials* **32**, 5515–5524 (2020).

[9] Luo, Z. *et al.* 0d $Cs_3Cu_2X_5$ (X = I, Br, and Cl) nanocrystals: Colloidal syntheses and optical properties. *Small* **16**, 1905226 (2020).

[10] Lu, Y., Fang, S., Li, G. & Li, L. Optimal colloidal synthesis and quality judgment of low-dimensional $Cs_3Cu_2Cl_5$ nanocrystals with efficient green emission. *Journal of Alloys and Compounds* **903**, 163924 (2022).

[11] Sadeghi, S. *et al.* Autonomous nanomanufacturing of lead-free metal halide perovskite nanocrystals using a self-driving fluidic lab. *Nanoscale* **16**, 580–591 (2024).

[12] Sui, J., Yan, J., Liu, D., Wang, K. & Luo, G. Continuous synthesis of nanocrystals via flow chemistry technology. *Small* **16**, 1902828 (2020).

[13] Jiang, Z. *et al.* Scale-up synthesis of high-quality solid-state-processed CsCuX (X = Cl, Br, I) perovskite nanocrystal materials toward near-ultraviolet flexible electronic properties. *RSC advances* **13**, 5993–6001 (2023).

[14] Lian, L. *et al.* Efficient and reabsorption-free radioluminescence in $Cs_3Cu_2I_5$ nanocrystals with self-trapped excitons. *Advanced Science* **7**, 2000195 (2020).

[15] Akkerman, Q. A. *et al.* Molecular iodine for a general synthesis of binary and ternary inorganic and hybrid organic-inorganic iodide nanocrystals. *Chemistry of Materials* **30**, 6915–6921 (2018).

[16] Hull, S. & Berastegui, P. Crystal structures and ionic conductivities of ternary derivatives of the silver and copper monohalides—ii: ordered phases within the $(AgX)_x$-$(MX)_{1-x}$ and $(CuX)_x$-$(MX)_{1-x}$ (M = K, Rb and Cs; X = Cl, Br and I) systems. *Journal of Solid State Chemistry* **177**, 3156–3173 (2004).

[17] Wyckoff, R. W. & Posnjak, E. The crystal structures of the cuprous halides. *Journal of the American Chemical Society* **44**, 30–36 (1922).

[18] Morlin, Z. Phase transformation of thin caesium iodide layers at low temperature. *Acta Crystallographica Section B: Structural Crystallography and Crystal Chemistry* **27**, 2493–2494 (1971).

[19] Gao, Y., Pinho, B. & Torrente-Murciano, L. Recent progress on the manufacturing of nanoparticles in multi-phase and single-phase flow reactors. *Current Opinion in Chemical Engineering* **29**, 26–33 (2020).

[20] Dlugosz, O. & Banach, M. Inorganic nanoparticle synthesis in flow reactors—applications and future directions. *Chemical Engineering* **5**, 1619–1641 (2020).

[21] Maceiczyk, R. M. *et al.* Microfluidic reactors provide preparative and mechanistic insights into the synthesis of formamidinium lead halide perovskite nanocrystals. *Chemistry of Materials* **29**, 8433–8439 (2017).

Acknowledgements

Author contributions

K.Arslanova and P.Ganswindt contributed equally to this manuscript. The manuscript was written through contributions of all authors. All authors have given approval to the final version of the manuscript.

Competing interests

The authors declare no competing interests.